Available online at www.sciencedirect.com
ScienceDirect
Journal of Power Sources 178 (2008) 323–333
JOURNAL OF POWER SOURCES
www.elsevier.com/locate/jpowsour

Coupling RTD and EIS modelling to characterize operating non-uniformities on PEM cathodes

Jonathan Deseure *

LEPMI, (UMR 5631), CNRS-INPG-UJF, 1130, rue de la piscine, ENSEEG, BP 75 38402 Saint Martin d'Hères, cedex France

Received 29 December 2006; received in revised form 23 November 2007; accepted 25 November 2007

Abstract

Large PEM cells will be used in future proton exchange membrane fuel cell (PEMFC) power plants and appropriate tools are therefore be needed to study their behaviour. One approach to understanding single cell behaviour involves using mathematical models. The numerous techniques used in this work to describe PEM electrode behaviour require different scientific disciplines: chemical engineering and electrochemistry. This study proposes combining residence time distribution (RTD) and electrochemical impedance spectroscopy (EIS). The investigation focuses on cathodic DC and AC responses where over-voltage is critical. Results demonstrate that although gas distribution does not cause additional loops on impedance diagrams, it is strongly related to both the shape and amplitude of these diagrams. The simulations have drawn attention to operating conditions that can threaten the life of the PEM cell: under these setting points EIS method is not sufficient to detect this risk.

Keywords: PEMFC modelling; Residence time distribution; Electrochemical impedance spectroscopy

1. Introduction

In recent years, fuel cell technology has attracted considerable attention from several fields of scientific research. Fuel cells are highly efficient in terms of energy produced, they emit little noise, and, if fed by hydrogen, are non-polluting. Fuel cell development is particularly important for stationary and portable applications. Amongst the several types of fuel cells, distinguished by their electrolyte, PEMFCs are often proposed because of their mild operating conditions (50–80 °C temperature, 1–3 atm pressure). PEMFCs are composed of a polymer electrolyte sandwiched between two porous backing layers to form a membrane electrode assembly (MEA). The electrodes (the active layers) are inserted between the electrolyte and the backing layers. One of the difficulties in characterising PEM electrodes is related to the scaling-up of the fuel cell. Thus, a specific approach must be developed for large PEM electrodes. A well-established powerful tool for investigating the mechanisms of physico-chemical and electrochemical reactions occurring at PEMFC electrodes is the electrochemical impedance spectroscopy (EIS). This method allows one to characterize an electrode behaviour under various conditions of flow feeding and applied current density. The purpose of this study is to combine the continuous stirred tank reactors (CSTR) approach with DC and AC electrochemical descriptions. Indeed, it is possible to improve IES explanations.

According to Bernardi and Verbruge [1] and Jaouen et al. [2], since water is produced at the cathode, the impact of water management on cathode performance is significant at high current densities. Nevertheless, these authors do not model mass transfer in the whole MEA. Experimental studies by Buchi and Srinivasan [3] confirmed the importance of gas hydration: ionic transport through the membrane is the most limiting phenomenon when gas humidification is low. However, Sena et al. [4] showed that the access of gases to catalytic surfaces becomes a limiting factor when the membrane is sufficiently hydrated. Costamagna and Srinivasan [5,6] and Okada et al. [7] confirmed these observations using steady state and transient modelling. Typically, the electrode (active layer) is sandwiched between the polymer membrane (Nafion®) and the gas diffusion layer (GDL). On both sides of the active layer, the mass balance in the GDL and the polymeric membrane is controlled by the gas flux inside the gas channel and the water flux through the MEA. Most models focus only on the cathode side of the fuel cell, because the

* Tel.: +33 476 82 67 33.
E-mail address: Jonathan.Deseure@lepmi.inpg.fr.

0378-7753/$ – see front matter © 2007 Elsevier B.V. All rights reserved.
doi:10.1016/j.jpowsour.2007.11.071

Nomenclature

b_i	Tafel slope, (V dec^{-1})
c_{H_2O}	water concentration, (mol m^3)
C_{dl}	double layer capacitance, (F m^{-2})
d_{pore}	pore diameter, (m)
D_{ij}	diffusion coefficient of species i through j, (m^2 s^{-1})
D_{ij}^{eff}	effective diffusion coefficient, (m^2 s^{-1})
D_m	effective diffusion coefficient of water in the membrane, (m^2 s^{-1})
D_i^p	Knudsen diffusion coefficient, (m^2 s^{-1})
EW	equivalent weight, (kg mol^{-1})
F	Faraday's constant, (C mol^{-1})
i	local current density, (A m^{-2})
i_f	Faradaic current density, (A m^{-2})
$i_{o(i)}$	exchange current density, (A m^{-2})
J	average current density, (A m^{-2})
L	thickness, (m)
M_i	molar weight, (kg mol^{-1})
N	density of molar flux, (mol m^{-2} s)
P	Pressure, (Pa)
P_{sat}	saturated vapour pressure, (Pa)
r_{O_2}	stoichiometry oxygen coefficient (-)
R	universal gas constant, (J mol^{-1} K^{-1}) (-)
S	electrode geometric area, (m^2)
t	time component, (s)
T	temperature, (K)
x	space component, (m)
X	electrode area ratio (-)
y_i	molar rate of the gas species i, (-)
Z	impedance (Ω m^2)

Greek symbols

ε	porosity, (-)
γ	roughness factor, (-)
η_i	overpotential, (V)
φ	density of molar flux, (mol m^{-2} s)
λ	water content in the membrane, (-)
ν	stoichiometric coefficient (-)
ρ_{dry}	dry Nafion® density, (kg m^{-3})
σ_{H^+}	protonic conductivity, (S m^{-1})
$\sigma_{H^+}^{eff}$	effective protonic conductivity, (S m^{-1})
τ	tortuosity, (-)
τ_o	osmotic coefficient, (mol mol^{-1})
ξ	liquid/gas flux ratio (-)
ψ_{Nafion}	agglomerate polymer content (-)

Indices and exposits

a	Anode
act	Active layers
b	Backing layers
c	Cathode
H_2	Hydrogen
H_2O	Water
k	Space discrete component
m	Membrane
n	Space discrete component
N_2	Nitrogen
O_2	Oxygen

cathode activation potential is the single largest source of inefficiency in fuel cells. Oxygen-reduction reaction at the cathode (1) is a key to PEMFC electrochemical behaviour:

$$O_2 + 4H^+ + 4e^- \rightarrow H_2O \quad (1)$$

The literature proposes various ways of predicting the electrochemical behaviour of electrodes. Thus, Springer et al. [8,9] proposed analytical formulations of EIS and emphasized the capacitive and resistive effects of oxygen reduction, and Eikerling and Kornyshev [10] complemented these steady state models with their descriptions of electrode microstructure. Studies conducted by Bultel et al. [11] showed that migration and diffusion processes play a crucial role in the active layer. Song et al. [12], by taking into account the multi-step reactions, have also shown the diffusion limitation occurring in the backing layer. The results of these studies [11,12] indicate that, on a complex plane plot (impedance diagram), diffusion limitation leads to a semi-circle at low frequencies, while ionic ohmic drop produces a straight line with a 45° angle at high frequencies, which is in agreement with Lasia's predictions [13,14]. Costamagna and Srinivasan [5,6] and Djilali et al. [15] have suggested that multidimensional modelling improves electrode description, since gas composition and temperature vary along the gas channels. In addition, these phenomena become critical for large cell areas. Under these conditions, recent investigations [16–19] have been carried out using computational fluid dynamics software. However, resolution in these approaches requires substantial computation time. Another simple way to describe the fluid dynamics is to use residence time distribution (RTD) techniques. Boillot et al. [20] have demonstrated that the bipolar plates are similar to a series of CSTRs, while Benziger et al. [21] have used the stirred tank reactor (STR) approach to explore the auto-humidification of the PEMFC. Furthermore, the RTD model does not require lengthy computing times.

The present study uses series of CSTRs based on RTD results obtained on PEM electrodes [20] and therefore the RTD technique is not investigated here. The purpose of this study is to combine the CSTR approach with more classical DC and AC electrochemical descriptions. AC behaviour is currently used to characterize the electrochemical generator: the electrochemical impedance spectroscopy technique. It is therefore important to accurately evaluate EIS responses. Thus, the aim of this study is to develop an approach to describe the behaviour of electrodes with a large surface area. This investigation takes into account Stefan–Maxwell diffusion process through the backing and catalyst layers [8] completed by a supplementary term for Knudsen diffusion in the small pores. In an earlier study, Ramousse et al. [22] presented a theoretical one-dimensional model in steady state. To complete this description of the PEM electrode, as well

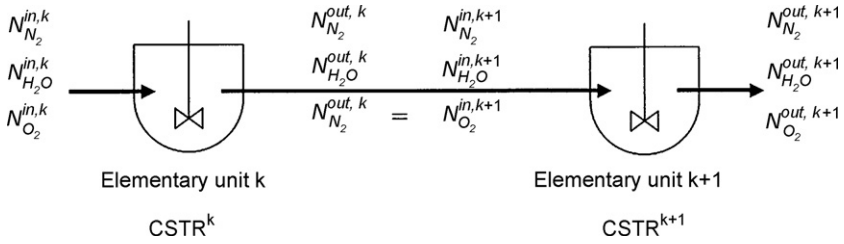

Fig. 1. Distribution of molar flux in elementary units (CSTR in series approach).

as that of the processes occurring therein, the present study proposes AC simulations. Moreover, the CTR approach presented here is applicable to one- or two-dimensional simulations [23].

2. Theory

On both sides of the MEA, the bipolar plates combine three functions: thermal control through cooling water channels, gas feeding via the gas channels, and current collector. The porous backing layers ensure a homogeneous gas distribution on the MEA. The active layers are thin layers of catalyst dispersed on carbon particles embedded in the polymer electrolyte. The catalysed electrochemical and chemical reactions occur in these layers. Only protons and water can go through the polymer membrane located at the centre of the assembly.

2.1. Gas channel model

The mass balance inside the gas channel is solved using a simplified fluid dynamic representation such as a CSTR [20] series. The electrode is divided into k elementary units. With such a hypothesis, gas transport in the gas channel is assumed to be infinitely fast, leading to homogeneous gas composition for each CSTR. In particular, the partial pressure of a component in the elementary unit (k) is equal to that of the outlet and to that of the elementary unit ($k+1$) inlet, as illustrated in Fig. 1.

All elementary units have the same voltage U due to the high electrical conductivity of bipolar plates and backing layers (GDL). This implies a current density distribution along the gas channel that is determined by local characteristics $J = f(U, P_{O_2}, P_{H_2}, P_{H_2O}, T)$. Thus, the partial pressures of each component in each elementary unit vary and make it necessary to solve mass balances and current densities in each elementary unit at the same time. The current voltage expression used is that proposed by our electrode model [22]. The molar balance equation of each CSTR with an electrode geometric area of S^k for each component in the gas phase in steady state, is written as:

$$\mathrm{N}_{\mathrm{H_2O}}^{k,\mathrm{in}} - \mathrm{N}_{\mathrm{H_2O}}^{k,\mathrm{out}} = \xi^k \mathrm{S}^k \varphi_{\mathrm{H_2O}}^k \tag{2}$$

$$\mathrm{N}_{\mathrm{O_2}}^{k,\mathrm{in}} - \mathrm{N}_{\mathrm{O_2}}^{k,\mathrm{out}} = \mathrm{S}^k \varphi_{\mathrm{O_2}}^k \tag{3}$$

$$\mathrm{N}_{\mathrm{N_2}}^{k,\mathrm{in}} - \mathrm{N}_{\mathrm{N_2}}^{k,\mathrm{out}} = 0 \tag{4}$$

and the global mass balance for each CSTR is given by:

$$\mathrm{N}_T^{k,\mathrm{in}} - \mathrm{N}_T^{k,\mathrm{out}} = \mathrm{S}^k(\varphi_{\mathrm{O_2}}^k + \varphi_{\mathrm{H_2O}}^k) \tag{5}$$

where $\mathrm{N}_\theta^x = y_\theta^x \mathrm{N}_T^x$, and the gas flux of consumption and production are expressed as follows:

$$\varphi_{\mathrm{H_2O}}^k = -\mathrm{N}_{\mathrm{H_2O}}^{\mathrm{membrane},k} + \frac{i^k}{2F} \tag{6}$$

$$\varphi_{\mathrm{O_2}}^k = -\frac{i^k}{4F} \tag{7}$$

The present work is conducted on the gas phase only and we have introduced ξ^k, representing the ratio of gas molar flux to liquid molar flux, which is estimated using a numerical optimisation ($1 \leq \xi^k \geq 0$). The saturated vapour pressure of water is expressed as follows:

$$P_{\mathrm{sat}} = e^{(23.1964 - (3816.44/T - 46.13))} \tag{8}$$

2.2. Electrode model

Srinivansan and Hurwirtz [24] assert that it is preferable to use a volumetric description of the active layer and a formalism of the Butler–Volmer type rather than a description derived from Tafel's law. The agglomerate model [25] that assumes the presence of macro-pores in the electrodes seems to be well adapted to the PEMFC anode and cathode. Siegel et al. [26] used it to simulate the electrochemical behaviour of a MEA.

Fig. 2 shows a schematic representation of the simplified pore structure assumed in the agglomerate model. The solid phase consists of a homogeneous mixture of polymer electrolyte (e.g. Nafion®), carbon, and catalyst (Pt). In the agglomerate, there is both an ionic current density flux and an electronic current density flux. These vary with the x coordinate. The ionic current density is nil at the active layer/backing layer interface ($x = 0$) and the electronic density is nil at the membrane/active layer interface ($x = L_{\mathrm{act}}$). In steady state, the local variation in electronic current density is the mathematical opposite of the local variation in ionic current density; it is also equal to the faradaic current density i_f. Cell current density J is the sum (over the electrode thickness L_{act}) of faradic current density:

$$i^k = \frac{\gamma}{L_{\mathrm{act}}} \int_0^{\mathrm{L_{act}}} i_f^k \mathrm{d}x \tag{9}$$

According to Kim et al. [27] the oxygen-reduction process is limiting. Boyer et al. [28] claim that the ionic conductivity

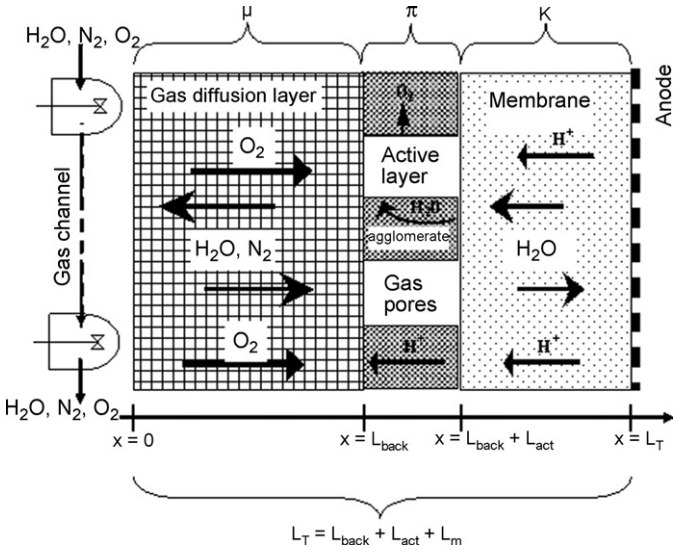

Fig. 2. Schematic description of the PEMFC half cell (cathode).

of the active layer influences the electrochemical performance of the electrodes. However, oxygen access to the catalyst sites remains problematic, not only because of the flooding risk, but also due to its low partial pressure. As Bernardi and Verbruge [1] proposed, a one-dimensional model can describe cathode operation by taking into account only the oxygen diffusion in the gas pores and the reduction kinetics. Under this condition, our main assumptions in the model are the following:

1. Mass transfer of H_2O and O_2 is considered only in the gas pores; there is no diffusion of water in the agglomerate.
2. H_2O concentration in the agglomerate is imposed by thermodynamic equilibrium with the gas phase.
3. The ionic conductivity of the agglomerate is a function of the ionic conductivity of the polymer, which depends on its water content.
4. Only the migration of protons is considered in the agglomerate.
5. Pressure and temperature are uniform.

Stefan–Maxwell equations [8], completed by a supplementary term for Knudsen diffusion in the small pores of the active layer and backing layer [22], describe the diffusion of hydrogen and water in the gas phase:

$$\frac{\mathrm{d}y_\theta^k}{\mathrm{d}x} = \frac{RT}{P}\left(\sum_\vartheta \left[\frac{y_\theta^k \varphi_\vartheta^k - y_\vartheta^k \varphi_\theta^k}{D_{\theta\vartheta}^{\mu,\pi}}\right] - \frac{\varphi_\theta^k}{D_\theta^p}\right) \tag{10}$$

The Knudsen diffusion coefficient D_i^p is expressed as follows:

$$D_i^p = d_{\mathrm{pore}}\frac{\tau}{3\varepsilon_{\mathrm{act}}}\sqrt{\frac{8RT}{\pi M_i}} \tag{11}$$

where $\varepsilon_{\mathrm{act}}$ is the porosity and τ the tortuosity of the active layer. The pore equivalent diameter (d_{pore}) can be estimated by [22]:

$$d_{\mathrm{pore}} = \frac{\varepsilon_{\mathrm{act}}}{1-\varepsilon_{\mathrm{act}}}\delta \tag{12}$$

Given that the inside of the backing layers is porous, it is necessary to use effective diffusion coefficients [22]:

$$D_{i,j}^{\mathrm{eff}} = \varepsilon_b^{2/3} D_{i,j} \tag{13}$$

$D_{i,j}$, the coefficient diffusions in the gas phase, come from [29]

Let us add: $\sum_\theta y_\theta^k = 1$ and the condition that only water can go through the membrane, in a direction depending on current density and gas hydration [7]. These are given by the following expressions:

$$\frac{\partial \varphi_\theta^k}{\partial x} = \frac{P}{RT}\frac{\partial y_\theta^k}{\partial t} \tag{14}$$

Oxygen consumption and water production in the porous active layer yield the following mass balance equations:

$$\frac{\partial \varphi_\theta^k}{\partial x} = \frac{p}{RT}\frac{\partial y_\theta^k}{\partial t} + \nu\frac{i_F}{nF} \tag{15}$$

where ν equals to 0 for nitrogen, −1 for oxygen and +1 for water.

The overpotential distribution Eq. (18) in the active layer can be calculated by means of the proton balance (16) and Ohm's law (17) in the ionic phase:

$$\frac{\partial i^k}{\partial x} = \frac{\gamma}{L_{\mathrm{act}}}\left(i_f^k + C_{\mathrm{dl}}\frac{\partial \eta^k}{\partial t}\right) \tag{16}$$

$$\frac{\partial \eta^k}{\partial x} = \frac{i^k}{\sigma_{\mathrm{H^+}}^{\mathrm{eff},k}} \tag{17}$$

$$\frac{\partial(\sigma_{\mathrm{H^+}}^{\mathrm{eff}}\partial\eta^k)}{\partial x^2} - \frac{\gamma}{L_{\mathrm{act}}}i_f^k = \frac{\gamma}{L_{\mathrm{act}}}C_{\mathrm{dl}}\frac{\partial \eta^k}{\partial t} \tag{18}$$

The effective ionic conductivity of the agglomerate depends on Nafion®'s conductivity and is simply corrected as a function of the agglomerate polymer content, as follows:

$$\sigma_{\mathrm{H^+}}^{\mathrm{eff}}(x) = \psi_{\mathrm{Nafion}}\sigma_{\mathrm{H^+}}(x) \tag{19}$$

The ionic conductivity of the membrane depends on its temperature and water content, according to this correlation [22]:

$$\sigma_{\mathrm{H^+}} = e^{(-E_{\mathrm{A}}(1/T-1/353))}(0.0013\lambda^3 + 0.0298\lambda^2 + 0.2658\lambda) \tag{20}$$

with

$$E_{\mathrm{A}} = 2640e^{(-0.6\lambda)} + 1183 \tag{21}$$

where the polymer water content λ is defined as the number of water moles per mole of sulfonic acid:

$$\lambda = \frac{\mathrm{EW}}{\rho_{\mathrm{dry}}}c_{\mathrm{H_2O}} \tag{22}$$

where EW (equivalent weight) represents the dry membrane weight per mole of the sulfonate group (kg mol^{-1}); ρ_{dry} is the

density of dry polymer (kg m^{-3}). The water content (λ) of the polymer electrolyte/gas interface assumes thermodynamic equilibrium between water vapour in the electrodes and liquid water in the polymer. The sorption curve of Hinatsu et al. [29] is:

$$\lambda = 0.3 + 10.8\left(\frac{p_{H_2O}}{P_{sat}}\right) - 16\left(\frac{p_{H_2O}}{P_{sat}}\right)^2 + 14.1\left(\frac{p_{H_2O}}{P_{sat}}\right)^3 \quad (24)$$

Thus, the agglomerate ionic conductivity is a function of the x co-ordinate. Finally, the Butler–Volmer law [22] is generally used to describe oxygen-reduction kinetics in acid media (e.g. Nafion®):

$$i_f^k = i_{0(O_2)}\left(e^{(2.3/b_{O_2}|\eta^k|)}\frac{y^k}{\overset{\circ}{y}_{O_2}} - e^{(-2.3/b^*|\eta^k|)}\right) \quad (25)$$

where $\overset{\circ}{y}_{O_2}$ is the hydrogen concentration at the inlet under open-circuit conditions.

2.3. Membrane model

The phenomenological model of water transport in the membrane proposed by Springer et al. [8] is used here. According to Okada et al. [7], the water electro-osmotic flux through the membrane, which is always directed from anode to cathode, is a linear function of the proton flux imposed by current density: The water diffusion flux through the membrane depends linearly on the water concentration gradient. The sum of diffusion and electro-osmotic fluxes yields a differential equation for the λ variable:

$$D_m\frac{\partial^2\lambda^k}{dx^2} = \tau_0\frac{i^k}{F}\frac{\partial\lambda^k}{\partial x} + \frac{\partial\lambda^k}{\partial t} \quad (26)$$

where τ_0 is the electro-osmotic drag coefficient and D_m the back diffusion coefficient [7].

2.4. DC solutions

The mass balance of CSTR series uses the following initial conditions: y_{O_2,N_2,H_2O}, and the results of the microscopic model (i^k, $N_{H_2O}^{membrane,k}$). The steady state equations of each elementary unit are solved using the simplex numerical optimisation method.

The resolutions of mass balances are numerically obtained thanks to the continuity of the flux between the backing layer, the active layer and the membrane. The boundary conditions of Eqs. (14) and (15) are given by the output of the mass balance in CSTR:

- concentration of each species at the gas channel/backing layer interface,
- molar flux density of oxygen and nitrogen are nil at membrane/electrode layer interface $\varphi^k_{N_2(x=L_{back}+L_{act})} = \varphi^k_{O_2(x=L_{back}+L_{act})} = 0$,
- molar flux density of water is given by the solution of the Eq. (28) $\varphi^k_{H_2O(x=L_{back}+L_{act})} = \varphi_{H_2O}^{membrane,k}$.

In steady state, the sum of diffusion and electro-osmotic fluxes (Eq. (26)) yields the following first-order differential equation:

$$\varphi_{H_2O}^{membrane,k} = \lambda^k\tau_0\frac{i^k}{F} - D_m\frac{\rho_{dry}}{EW}\frac{d\lambda^k}{dx} \quad (27)$$

The solution of Eq. (27) is:

$$\varphi_{H_2O}^{membrane,k} = \frac{\tau_0 i^k}{F}\left[\lambda_a + \frac{\lambda_c^k - \lambda_a^k}{1-\exp(k_m^k L_m)}\right] \quad (28)$$

with

$$k_m^k = \frac{EW\tau_0 i^k}{\rho_{dry}D_m F}.$$

λ_c^k and λ_a^k stand for the polymer water content at the membrane/active layer interface. Then, assuming thermodynamic equilibrium between water vapour in the backing layers and liquid water in the polymer, the sorption curve of Hinatsu et al. [7], Eq. (24) is used to relate partial pressure values to λ_c^k and λ_a^k.

In steady state, the solution of Eq. (18) describes the distributions of concentrations and electrode overpotentials as functions of x coordinate. This differential equation has to be solved with the following boundary conditions:

- Ionic current density is nil at the active layer/backing layer interface $-\sigma_{H^+}^{eff}\,d\eta/dx|_{x=L_{back}} = 0$.
- Electrode overpotential at the membrane/active layer interface is known: $\eta_{(x=L_{back}+L_{act})} = \eta_0$. In practice, η_0 is adjusted until J equals the value used for the determination of hydrogen consumption (29).

This set of equations is solved by iterative methods and only needs the following inlet conditions: $\overset{\circ}{y}_{O_2}$, $\overset{\circ}{y}_{N_2}$, $\overset{\circ}{y}_{H_2O}$ and $N_{N_2}^{in,0}$,$N_{H_2O}^{in,0}$,$N_{O_2}^{in,0}$ where $N_{N_2}^{in,0} = y_{O_2}^* N_T^{in,0}$. The conventional way of investigating the influence of mass flux on electrochemical behaviour is by using the inlet molar fluxes, which are proportional to the current density and the stoichiometry, for the cathode such that:

$$N_{O_2}^{in,0} = S^T\frac{\chi_{O_2}}{\overset{\circ}{y}_{O_2}}\frac{J}{4F} \quad (29)$$

where J is the average current density of i^k and S^T the total geometric area of electrode $S^T = \sum_k S^k$. In this study, the initial inlet molar flux density $N_{O_2}^{in,0}$ is fitted to the case where there is only one CSTR.

2.5. AC solutions

When a small sinusoidal amplitude modulation Δi is added to the applied current density i, the concentrations of species

in solution or adsorbed are also modulated in a sinusoidal way around their steady state values. Under this condition, the faradaic current density could be expressed by:

$$\Delta i_f^k = i_f^k(t) - i_f^k = \partial_\eta i_f^k \Delta\eta^k(t) + \partial_{y_{O_2}} i_f^k \Delta y_{O_2}^k(t) \quad (30)$$

where $\partial_\eta i_f$, $\partial_\theta i_f$ et $\partial_V i_f$ are the partial derivatives of the faradaic current density calculated at the steady state such that:

$$\partial_\eta i_f = \left.\frac{\partial i_f}{\partial \eta_c}\right|_{y_{O_2}} = \frac{i_{O(O_2)}}{b_{O_2}} 2.3 \left(e^{2.3/b_{O_2}|\eta_{ci}|} \frac{y_{O_2}}{\overset{\circ}{y}_{O_2}} + \frac{b_{O_2}}{b^*} e^{-2.3/b^*|\eta_c|} \right) \quad (31)$$

$$\partial_{y_{O_2}} i_f = \left.\frac{\partial i_f}{\partial y_{O_2}}\right|_{\eta_a} = \frac{i_{0(O_2)}}{\overset{\circ}{y}_{O_2}} e^{2.3/b_{O_2}|\eta_c|} \quad (32)$$

We denote Laplace transforms (introducing $s = j\omega$ where ω is the angular frequency) of the time-dependent perturbed variables with an overbar.

$$\Delta \bar{i}_f^k = \partial_{y_{O_2}} i_f^k \Delta \bar{y}_{O_2}^k + \partial_\eta i_f^k \Delta \bar{\eta}^k \quad (33)$$

Due to this same variation in the cathodic overpotential, after Laplace transforms Ohm's law can be written for any point of the active layer as follows:

$$\frac{d\Delta\bar{\eta}^k}{dx} = \frac{\Delta \bar{i}^k}{\sigma_{H^+}^{\text{eff},k}} \quad (34)$$

and the proton balance can be expressed by:

$$\frac{d\Delta\bar{i}^k}{dx} = \frac{\gamma}{L_{\text{act}}} (\Delta\, \bar{i}_f^k + s\, C_{\text{dl}} \Delta\bar{\eta}^k) \quad (35)$$

To solve this system numerically with simple discretization, we use a constant step size h. The discreet solution may be written as:

$$Z_n^k = \frac{L_{\text{act}}}{\sigma^{\text{eff},k}}\, h + \frac{1}{1/Z_{n-1}^k + \gamma\, h\, (1/Z^k + s\, c_{\text{dl}})} \quad (36)$$

where $Z_n^k = \Delta\bar{\eta}_n^k / \Delta\bar{i}_n^k$ is the local impedance at n active layer abscise and $Z_{f_n}^k = \Delta\bar{\eta}_n^k / \Delta\bar{i}_{f_n}^k$ the faradic impedance at n. The total impedance of the electrode can be represented in the form of a line transfer [19,10,11], Under these same conditions, the mass Eqs. (8)–(14) become:

$$\frac{d\Delta\bar{y}_\theta^k}{dx} = \frac{RT}{P} \left(\sum_\vartheta \left[\frac{(\varphi_\vartheta^k \Delta\bar{y}_\theta^k + y_\theta^k \Delta\bar{\varphi}_\vartheta^k) - (\varphi_\theta^k \Delta\bar{y}_\vartheta^k + y_\vartheta^k \Delta\bar{\varphi}_\theta^k)}{D_{\theta\vartheta}^{\mu,\pi}} \right] - \frac{\Delta\bar{\varphi}_\theta^k}{D_\theta^p} \right) \quad (37)$$

This equation of diffusion transport in the Laplace domain confirms that $\sum_\theta \Delta\bar{y}_\theta^k = 0$. The mass balance inside the GDL is expressed as follows:

$$\frac{d\Delta\bar{\varphi}_{N_2}^k}{dx} = s\frac{P}{RT} \Delta\bar{y}_{N_2}^k \quad (38)$$

The variation of oxygen consumption and water production in the porous active layer yield the following mass balance equations:

$$\frac{d\Delta\bar{\varphi}_{O_2}^k}{dx} + \frac{\gamma}{L_{\text{act}}} \frac{\Delta\bar{i}_f^k}{4F} = s\frac{P}{RT} \Delta\bar{y}_{O_2}^k \quad (39)$$

These ordinary differential equations have to be solved in the Laplace domain with the following boundary conditions:

- at the backing layer/gas channel interface, the variation in concentrations is nil due to the assumption of infinitely fast mixing, leading to an homogeneous gas composition (CSTR assumptions) $\Delta\bar{y}_{O_2(x=0)}^k = \Delta\bar{y}_{N_2(x=0)}^k = \Delta\bar{y}_{H_2O(x=0)}^k = 0$,
- at the active layer/membrane interface, the flux variation is nil for the oxygen and nitrogen $\Delta\bar{\varphi}_{N_2(x=L_{\text{back}}+L_{\text{act}})}^k = \Delta\bar{\varphi}_{O_2(x=L_{\text{back}}+L_{\text{act}})}^k = 0$,
- according to steady state boundary conditions, the flux variation of the water at the active layer/membrane interface is determined by $\Delta\bar{\varphi}_{H_2O(x=L_{\text{back}}+L_{\text{act}})}^k = \Delta\bar{\varphi}_{H_2O}^{\text{membrane},k}$.

According to Okada et al. [7], the variation of membrane water content in the Laplace domain involves the following expression for water transport:

$$s\Delta\bar{\lambda}^k = D_m \frac{\partial^2 \Delta\bar{\lambda}^k}{\partial x^2} - \tau_0 \left(\frac{i^k}{F} \frac{\partial \Delta\bar{\lambda}^k}{\partial x} + \frac{\partial \lambda^k}{\partial x} \frac{\Delta\bar{i}^k}{F} \right) \quad (40)$$

and the variation of water transport at this interface results in the sorption equilibrium such that:

$$\frac{\Delta\bar{\lambda}_c^k}{\Delta\bar{y}_{H_2O(x=L_{\text{back}}+L_{\text{act}})}^k} = K(T) \quad (41)$$

In order to determine the impedance of each elementary electrode (Z^k), the active layer was divided into n elements (length h), where n varies from 500 to 1000. Thus, the total impedance is given by:

$$\frac{1}{Z} = \frac{S^T}{S^k} \sum_k \frac{1}{Z^k} \quad (42)$$

To simulate the EIS, various inlet fluxes are investigated under many different levels of relative humidity. But the most important contribution of this study is the description of fluid dynamics made possible through the use of CSTR models. Different architectures are investigated with a view to predicting AC electrode behaviour: series and parallel pathways of CSTR.

3. Results and discussion

The values of selected parameters used to simulate both DC and AC behaviour are listed in Table 1. Most of them are based on data from the literature. The range selected for kinetic constants was chosen in order to obtain cathodic current densities similar to those observed in the PEMFC cathode (for $|\eta_c| = 0.55$ V, $J < 1$ A m^{-2}).

In this study, three kinds of humidification modes are investigated: auto-humidification, humidification of inlet gas and humidification via the membrane. Moreover, the inlet gas flux

Table 1
Simulation values

Parameter	Value	Refs.
L_{back}	230×10^{-6} m	[22]
L_{act}	10×10^{-6} m	[22]
L_m	125×10^{-6} m	[22]
ε_{back}	0.8	[22]
ε_{act}	0.3	[22]
ψ_{Nafion}	0.5	[22]
δ	3×10^{-6} m	[26]
ξ	1.7-	[22]
γ	$100\,m^2\,m^{-2}$	[30]
$b_{O_2} = b^*_{O_2}$	120 mV dec^{-1}	[30]
$i_{0(O_2)}$	4×10^{-7} A cm^{-2}	[30]
ε_m	0.28	[22]
EW	1.1 kg mol^{-1}	[7]
ρ_{dry}	2020 kg m^{-3}	[7]
τ_0	2.5/22-	[7]
D_m	3×10^{-10} m^2 s^{-1}	[7]
D_{O_2}/H_2O	3.20×10^{-5} m^2 s^{-1}	[22]
D_{O_2}/N_2	2.41×10^{-5} m^2 s^{-1}	[22]

also affects the electrochemical behaviour of the PEMFC cathode. This flux is currently expressed using the stoichiometry oxygen coefficient, expressed as follows:

$$r_{O_2} = 4F\frac{N^{in,0}_{O_2}}{S^T J} \tag{43}$$

The model presented here does not take into account the appearance of liquid water. Based on this assumption, the values of r_{O_2} are estimated in order to obtain a gaseous condition in the set of calculated cases. A simple mass balance [31] could be used to estimate the minimum flux of air or the r_{O_2} value for the non-appearance of liquid water on the cathode:

$$r_{O_2}(T) = 0.21\left[\frac{2 + P/P - P_{sat}(T)}{P/P - P_{sat}(T) - RH_C P/P - RH_C P_{sat}(T)}\right] \tag{44}$$

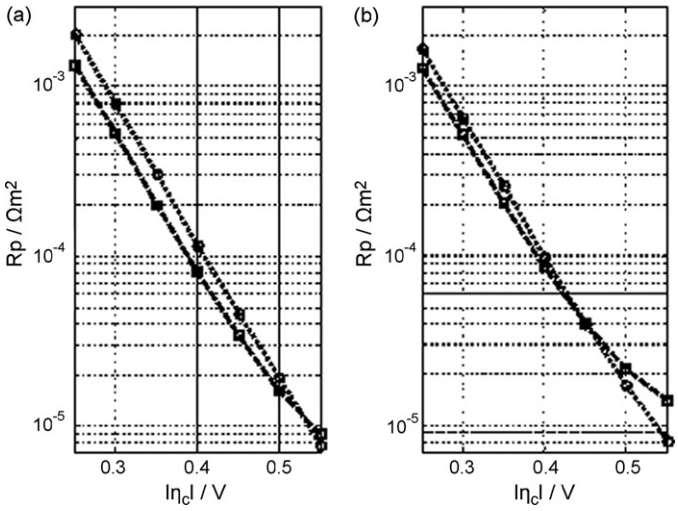

Fig. 3. Simulated polarisation resistance as a function of r_{O_2} for dry conditions, (a) 1 CSTR, (b) 20 CSTR with (◯), $r_{O_2} = 2.2$; (□), $r_{O_2} = 11$.

The limit of liquid water appearance depends on the relative humidity (RH_C) of inlet gas. This mass balance equation considers that the water produced by oxygen reduction is totally evacuated by the gas flux. This relationship does not take into account the water flux provided from the anode side: for this reason, a high stoichiometry oxygen coefficient is proposed. The selected values of $r_{O_2} = 2.2$ and 11 should avoid flooding at 60 °C for any simulated cases such as $RH_C < 0.8$ and $RH_C < 0.98$.

3.1. Electrochemical behaviour using dry inlet conditions

The following simulations show the effects of two phenomena: first, the inlet gas flux impact and second, the influence of gas distribution on the electrode. The effects of gas distribution are investigated using the CSTR description: for each CSTR, there is a corresponding uniform electrode zone. In Figs. 3 and 4,

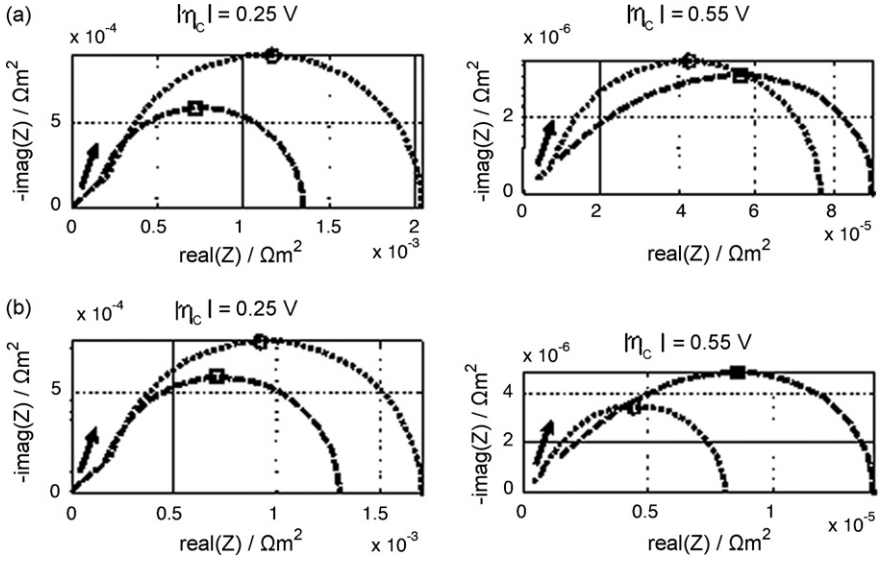

Fig. 4. Simulated complex impedance diagrams as a function of r_{O_2} for dry conditions at $|\eta_c| = 0.25$ V and $|\eta_c| = 0.55$ V, (a) 1 CSTR, (b) 20 CSTR with (◯), $r_{O_2} = 2.2$; (□), $r_{O_2} = 11$. The arrows indicate decreasing frequency values from 100 kHz to 10^{-3} Hz.

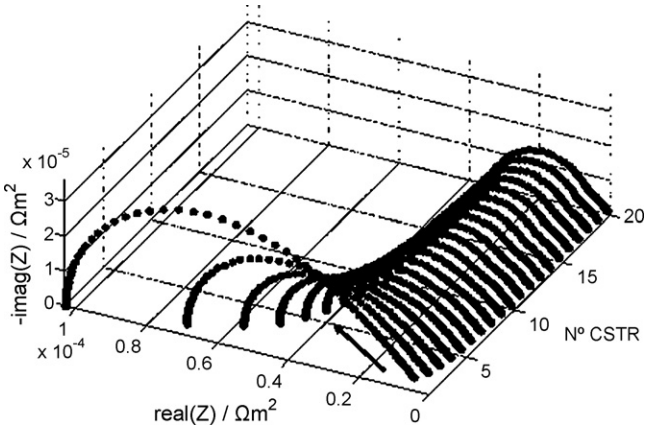

Fig. 5. Simulation of local impedance diagrams r_{O_2} for dry conditions with $|\eta_c| = 0.4$ V and $r_{O_2} = 11$. The arrow indicates decreasing frequency values from 100 kHz to 10^{-3} Hz.

the simulation of polarisation resistances or impedance diagrams demonstrates the competition between proton and oxygen access to the catalyst. The impedance diagram exhibits the shape of finite length diffusion impedance when proton access controls electrochemical performance [13] and that of a semi-circle when oxygen access controls performance [11]. In the case of a cathode with operating uniformity (CSTR = 1), the limiting transport step is oxygen diffusion: the impedance diagram exhibits a semi-circle shape at low frequencies, decreasing with the increasing stoichiometry oxygen coefficient ($|\eta_c| = 0.25$ V, Fig. 4a). The proton limitation could appear only at high current densities with a high inlet air flux: a 45° straight line in Fig. 4a ($|\eta_c| = 0.55$ V). For electrodes with operating non-uniformities (e.g. 20 CSTR), the analysis is similar to low cathodic over-voltage ($|\eta_c| = 0.25$ V, Fig. 4b). But at high current densities ($|\eta_c| = 0.4$ V, Fig. 3b), proton access becomes critical, which is confirmed by increasing electrode resistance as the stoichiometry oxygen coefficient increases (Fig. 4b, $|\eta_c| = 0.55$ V).

A study of local impedance is necessary to understand this behaviour. Local impedance diagrams are shown in Figs. 5 and 6. The CSTR are designated as 1–20 from the inlet gas to outlet gas. These figures are selected to highlight ionic transport (a 45° straight line) and oxygen transport (capacitive loop at low frequencies). In both figures, the impedance diagrams for the first CSTRs reflect the dry electrode effects. Thus, these zones do not produce enough water to satisfy the humidification requirements of the catalytic layer. However, subsequent zones receive more humidity.

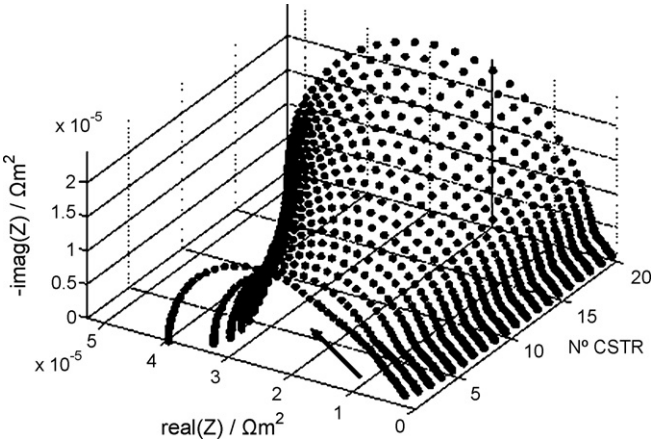

Fig. 6. Simulation of local impedance diagrams r_{O_2} for dry conditions with $|\eta_c| = 0.4$ V and $r_{O_2} = 2.2$. The arrow indicates decreasing frequency values from 100 kHz to 10^{-3} Hz.

Fig. 5 demonstrates that oxygen access does not constitute a limitation, and that electrochemical performance is limited more by proton access. Under these conditions, proton access is improved along the gas channel ($r_{O_2} = 11$) and local impedance decreases from the inlet to the outlet, gradually becoming constant. These simulation results are similar to the experimental observations of Schneider et al. [32], obtained using a local electrochemical impedance technique. But for $r_{O_2} = 2.2$ (Fig. 6), only the inlet zone exhibited limitation by proton access, due to the dry inlet conditions. The other zones exhibited limitation by oxygen access (low-frequency semi-circle). In addition, this capacitive contribution increases along the gas channel due to the consumption of oxygen.

At this point in the investigation, it is important to understand the influence of the CSTR description. This method results from the dynamical analysis of the gas distribution in the bipolar plates [20]. The following simulations underline the dependence of AC responses on CSTR modelling.

The simulations shown in Fig. 7 demonstrate that the impact of flux distribution on the electrode is a function of CSTR description. In this figure, two cases are proposed: low inlet flux of air ($r_{O_2} = 2.2$) and high inlet flux of air ($r_{O_2} = 11$).

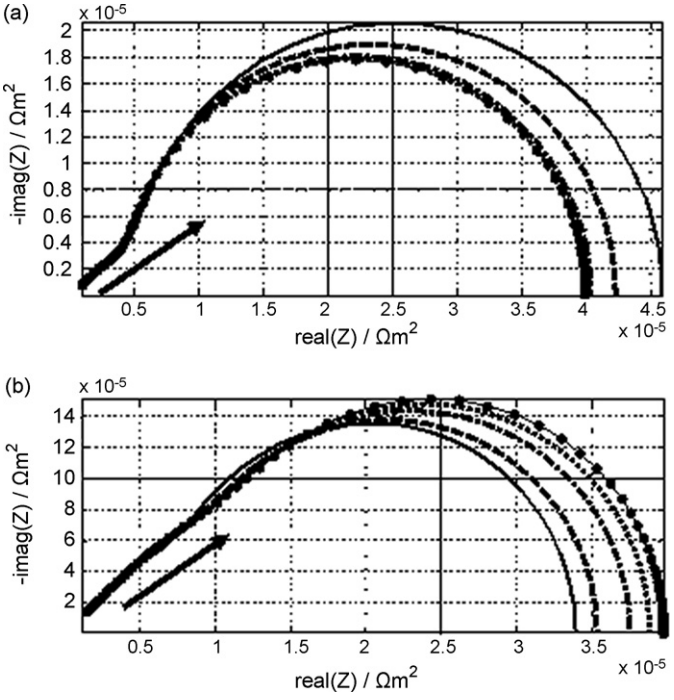

Fig. 7. Simulated complex impedance diagrams as a function of CSTR description for dry conditions with (a) $r_{O_2} = 2.2$ and (b) $r_{O_2} = 11$, $|\eta_c| = 0.45$ V (the arrow indicates an increasing number of CSTR descriptions). (—), 1 CSTR; (- -), 2 CSTR; (- -), 5 CSTR, (. . .), 10 CSTR and (●), 20 CSTR. The arrow indicates decreasing frequency values from 100 kHz to 10^{-3} Hz.

With a high air flux (Fig. 7(b)), the inlet zones do not produce enough water to ensure a correct level of humidification: the water produced is moved out of the cell too quickly, as shown in Fig. 5. This phenomenon is amplified by increasing the number of homogenous zones: increasing of drying zones. Thus, proton migration into the active layer could control the oxygen-reduction process, as observed by Jaouen et al. [2,33]. On the other hand, at low inlet flux levels the limiting process becomes gas access, as shown in Fig. 6. Thus, in Fig. 7a, the impedance diagrams decrease as the number of homogenous zones increases due to better oxygen access in the inlet zones. In these conditions, a progressive distribution of reactant on electrodes (20 CSTR) improves electrochemical performance.

3.2. Influence of humidification mode on EIS

The auto-humidification of the electrode was studied in the Section 1 of this paper, but the humidification modes of PEM electrodes also have an impact on IES. Three types of humidification are investigated in this study:

1. auto-humidification, extensively discussed in Section 3.1 where there is both a dry inlet gas and dry conditions at the anode/membrane interface,
2. humidification of inlet gas at half the saturated water pressure and dry conditions at the anode/membrane interface,
3. non-humidification of inlet gas but the anode/membrane interface is saturated by the water.

The 45° straight line appears at high frequencies for high feed fluxes and high current densities (Fig. 8). However, the change in shape of the impedance diagrams is faster for 10 CSTR than for 1 CSTR. This behaviour is linked to the existence of dry local effects that were presented in Figs. 5 and 6. Of course, the apex frequencies increase with over-voltage, but. the value of these frequencies depends on the inlet gas flux and on humidification modes. In case n°2 for $|\eta_c| = 0.25$ V, the value of the apex frequency increases from 14 Hz ($r_{O_2} = 2.2$) to 22 Hz ($r_{O_2} = 11$), while in case n°1 for $|\eta_c| = 0.25$ V, this value increases from 17 Hz ($r_{O_2} = 2.2$) to 29 Hz ($r_{O_2} = 11$). This observation underlines the competition between gas access (low frequencies) and proton access (high frequencies).

Hydration of the cathode via the anode side (case n°3) produces a special effect. Under this condition, the electro-osmotic flux is added to the back diffusion flux. Oxygen diffusion through the cathode slows down with the increasing water flux (Eq. (37)), according to the following ratio:

$$\frac{\varphi^k_{H_2O}\Delta\overline{y}^k_{N_2\text{ or }O_2}}{D^{\mu,\pi}_{H_2O,N_2\text{ or }O_2}} \tag{45}$$

This phenomenon corresponds to an increasing semi-circle in the impedance diagram. In general, humidification improves electrochemical performance and minimizes the effect of the oxygen stoichiometric coefficient (r_{O_2}).

3.3. Influence of flux distribution on EIS

In this section, a parallel pathway for the gas flux is investigated (Fig. 9). A new operating condition is proposed: the temperature is set at 65 °C to ensure total consumption of the oxygen and better steam transport ($P^{T=65°C}_{H_2O,sat} \approx 0.21$ atm). To understand the effects of gas distribution on the PEM electrode (case of parallel pathways), an additional parameter is added (Eq. (46)). In an earlier section of this work (Section 3.1), all CSTRs had the same electrode area, while in this section, the area of each CSTR is deduced from the following expression:

$$X^k_S = \frac{S^k}{S} \times 100 \tag{46}$$

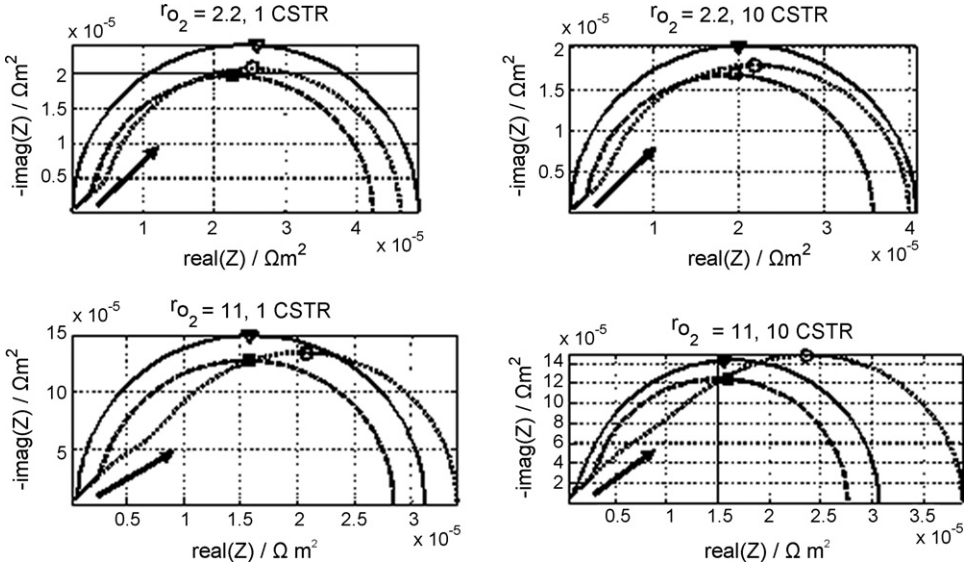

Fig. 8. Simulated complex impedance diagrams as a function of humidification conditions 8 for $|\eta_c| = 0.45$ V, with $r_{O_2} = 2.2$ and 11; (–□–), humidification of inlet gas at 1/2 of the saturated water pressure; (⊩-), water-saturated anode; (◯), auto-humidification (dry conditions). The arrow indicates decreasing frequency values from 100 kHz to 10^{-3} Hz.

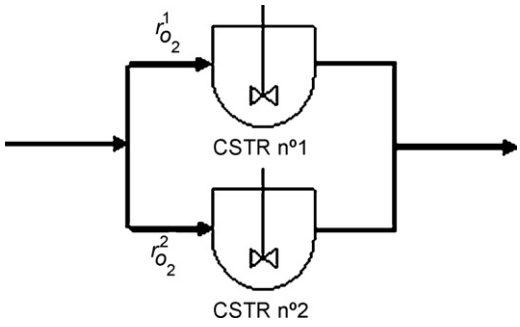

Fig. 9. Molar flux distribution in elementary units (CSTR).

In this section, we consider two CSTRs such as $1 = X^1_S + X^2_S$ to simulate a threat to the life of the PEM cell due to gas distribution. Thus, the simulation conditions are as follows:

- $r^1_{O_2} = 11$ (principal gas pathway),
- $r^2_{O_2} \approx 1$ such as $y^2_{O_2} \approx 10^{-5}$ (case of electrode dead zones),
- on both CSTRs, the inlet gas is dry,
- the anode side of CSTR n°1 is saturated by the water (case of water accumulation in dead end mode of fuel feed).

Fig. 10 shows the effect of current density distribution on polarisation resistances. As expected, polarisation resistance increases with increasing X^2_S area. Although the most important part of the current is provided by CSTR n°1, CSTR n°2 affects not only the value of polarisation resistance but also the shape of the impedance diagrams (Fig. 11): in Fig. 11 the 45° straight line disappears for $X^1_S = 60\%$. Under these conditions, it is difficult to observe local drying using the EIS technique. On the other hand, when liquid water is accumulated inside the electrode, the limiting diffusion could result in an additional low frequency contribution being observed in the impedance diagram: flooded electrode [14], or low electrode porosity [23]. Thus, it is possible that hazardous operating conditions cannot always be estimated.

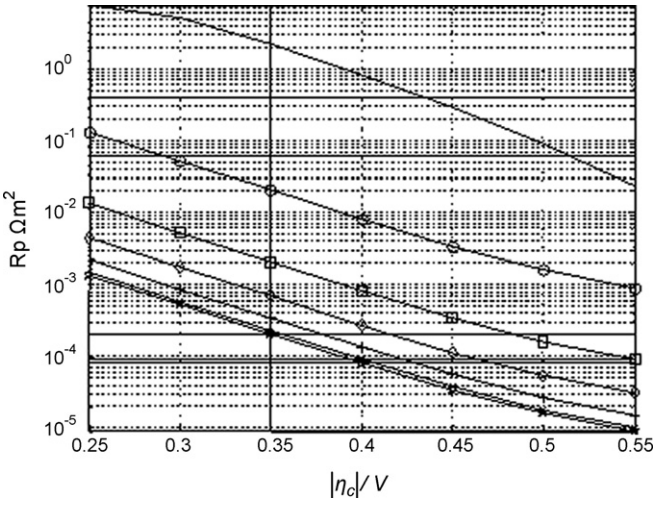

Fig. 10. Simulated polarisation resistances as a function of X^1_S. (—), $X^1_S = 0\%$; (◯), $X^1_S = 1\%$; (□), $X^1_S = 10\%$; (◇), $X^1_S = 30\%$, + $X^1_S = 60\%$; (×), $X^1_S = 90\%$; (☆), $X^1_S = 100\%$.

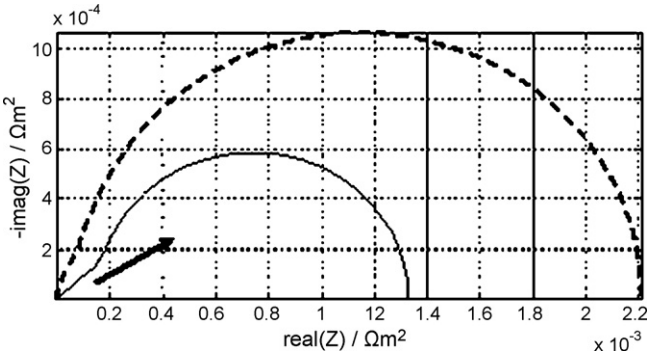

Fig. 11. Simulated complex impedance diagrams as a function of X^1_S and over-voltage. — 1 ($X^1_S = 100\%$ and $|\eta_c| = 0.25$ V), - - ($X^1_S = 60\%$ and $|\eta_c| = 0.25$ V), The arrow indicates decreasing frequency values from 100 kHz to 10^{-3} Hz.

4. Conclusion

Simulations are conducted only in the gas phase with a view to determining the impact of gas distribution in the gas channel on impedance diagrams. This work has presented the theoretical bases for an experimental method for characterising large PEM electrodes using the RTD method (CSTR model) coupled with IES techniques (AC model). Thus, to improve IES explanations, it is necessary to understand gas distribution. This approach does not require lengthy computations and the simulations are easier to fit to experimental data. In all the simulations, only one capacitive contribution is observed. Theoretically, AC active layer behaviour involves only one capacitive loop and an additional one due gas access through backing layer could not appear (large porosity $\varepsilon = 0.8$). Fluid distribution does not provide an additional loop but the changing shape is strongly linked to the CSTR description. So, it is difficult to observe local drying or flooding using the EIS technique alone. Moreover, operating conditions that can threaten the life of the PEM cell are not easy to detect using only the EIS method. Thus, this work has drawn attention to the relative advantages of using a fluid dynamics description coupled with the EIS technique. In the future, it will be important to include the flooding or partial flooding effects that were not taken into account in this study.

Acknowledgments

This work was financially supported by the CNRS. I gratefully acknowledge the contribution of many fruitful theoretical discussions with Mathieu Boillot and François Lapicque. I am also thankful to Olivier Lottin and Sophie Didierjean for providing a scientific overview.

References

[1] D.M. Bernardi, M.W. Verbruge, AIChe J. 37 (1991) 1151–1163.
[2] F. Jaouen, G. Lindbergh, G. Sundholm, J. Electrochem. Soc. 149 (4) (2002) A437–A447.
[3] F.N. Buchi, S. Srinivasan, J. Electrochem. Soc. 144 (1997) 2767–2772.
[4] D.R. Sena, E.A. Ticianelli, V.A. Paganin, E.R. Gonzalez, J. Electroanal. Chem. 477 (1999) 164–170.
[5] P. Costamagna, Chem. Eng. Sci. 56 (2001) 323–332.

[6] P. Costamagna, S. Srinivasan, J. Power Sources 102 (2001) 239–253.
[7] T. Okada, G. Xie, Y. Tanabe, J. Electroanal. Chem. 413 (1996) 49–65.
[8] T.E. Springer, T.A. Zawodzinski, M.S. Wilson, S. Gottesfeld, J. Electrochem. Soc. 143 (1996) 587–599.
[9] T.E. Springer, I.D. Raistrick, J. Electrochem. Soc. 136 (1989) 1594–1603.
[10] M. Eikerling, A.A. Kornyshev, J. Electroanal. Chem. 500 (2001) 30–31.
[11] Y. Bultel, L. Genies, O. Antoine, P. Ozil, R. Durand, J. Electroanal. Chem. 527 (2002) 143–155.
[12] H.K. Song, Y.H. Jung, K.H. Lee, L.H. Dao, Electrochim. Acta 44 (1999) 3513–3519.
[13] A. Lasia, J. Electroanal. Chem. 397 (1995) 27–33.
[14] A. Lasia, J. Electroanal. Chem. 500 (2001) 30–35.
[15] N. Djilali, D. Lu, Int. J. Therm. Sci. 41 (2002) 29–40.
[16] A. Kumar, R.G. Reddy, J. Power Sources 114 (2003) 54–62.
[17] S. Mazumder, J.V. Cole, J. Electrochem. Soc. 150 (11) (2003) A1503–A1509.
[18] S. Mazumder, J.V. Cole, J. Electrochem. Soc. 150 (11) (2003) A1510–A1517.
[19] W. Ying, Y.-J. Sohn, W.-Y. Lee, J. Ke, C.-S. Kim, J. Power Sources 145 (2005) 563–571.
[20] M. Boillot, S. Didierjean, F. Lapicque, Chem. Eng. Sci. 60 (2005) 1187–1192.
[21] J. Benziger, E. Chia, J.F. Moxley, L.G. Kevrekidis, Chem. Eng. Sci. 60 (2005) 1743–1759.
[22] J. Rammousse, J. Deseure, O. Lottin, S. Didierjean, D. Maillet, J. Power Sources 145 (2005) 416–427.
[23] M. Bautista, Y. Bultel, P. Ozil, Chem. Eng. Res. Des. 82 (2004) 907–917.
[24] S. Srinivasan, H.D. Hurwirtz, Electrochem. Acta 12 (1967) 495–512.
[25] F. Gloaguen, P. Convert, S. Gamburzev, O.A. Velev, S. Srinivasan, Electrochim. Acta 43 (1998) 3767–3772.
[26] N.P. Siegel, M.W. Ellis, D.J. Nelson, M.R. von Spakovsky, J. Power Sources 115 (2003) 81–89.
[27] J. Kim, S.-M. Lee, S. Srinivasan, C.E. Chamberlin, J. Electrochem. Soc. 142 (8) (1995) 2670–2674.
[28] C. Boyer, S. Gamburzev, O. Vlev, S. Srinivasan, A.J. Appleby, Electrochim. Acta 43 (1998) 3703–3709.
[29] J.T. Hinatsu, M. Mizuhata, H. Takenaka, J. Electrochem. Soc 141 (1994) 1493–1498.
[30] O. Antoine, Y. Bultel, R. Durand, P. Ozil, Electrochim. Acta 43 (1998) 3681–3691.
[31] R. Eckl, W. Zehtner, C. Leu, U. Wagner, J. Power Sources 138 (2004) 137–144.
[32] A. Schneider, H. Kuhn, A. Wokaun, G.G. Scherer, J. Electrochem. Soc. 152 (2005) A2383–A2389.
[33] F. Jaouen, G. Lindbergh, K. Wiezell, J. Electrochem. Soc. 150 (2003) A1711–A1717.